Electronic Supplementary Material (ESI) for Physical Chemistry Chemical Physics.
This journal is © the Owner Societies 2015

Electronic Supplementary Information

for

Intramolecular charge transfer character in tetrathiafulvalene-annulated porphyrinoids: Effects on core modification and protonation

Ramababu Bolligarla[a], Masatoshi Ishida[*,b], Vijayendra S. Shetti,[c] Kazuhisa Yamasumi[b], Hiroyuki Furuta[b], and Chang-Hee Lee*[*,a]*

[a]*Department of Chemistry, Kangwon National University, ChunCheon 200-701, Korea*

[b]*Department of Chemistry and Biochemistry, Graduate School of Engineering and Education Center for Global Leaders in Molecular Systems for Devices, Kyushu University 744 Motooka, Nishi-ku, Fukuoka, 819-0395, Japan*

[c] *Department of Chemistry, BMS College of Engineering, Bull Temple Road, Bangalore 560019, India*

CORRESPONDING AUTHORS

E-mail: chhlee@kangwon.ac.kr (C.-H. L.); ishida@molecular-device.kyushu-u.ac.jp (M.I.)

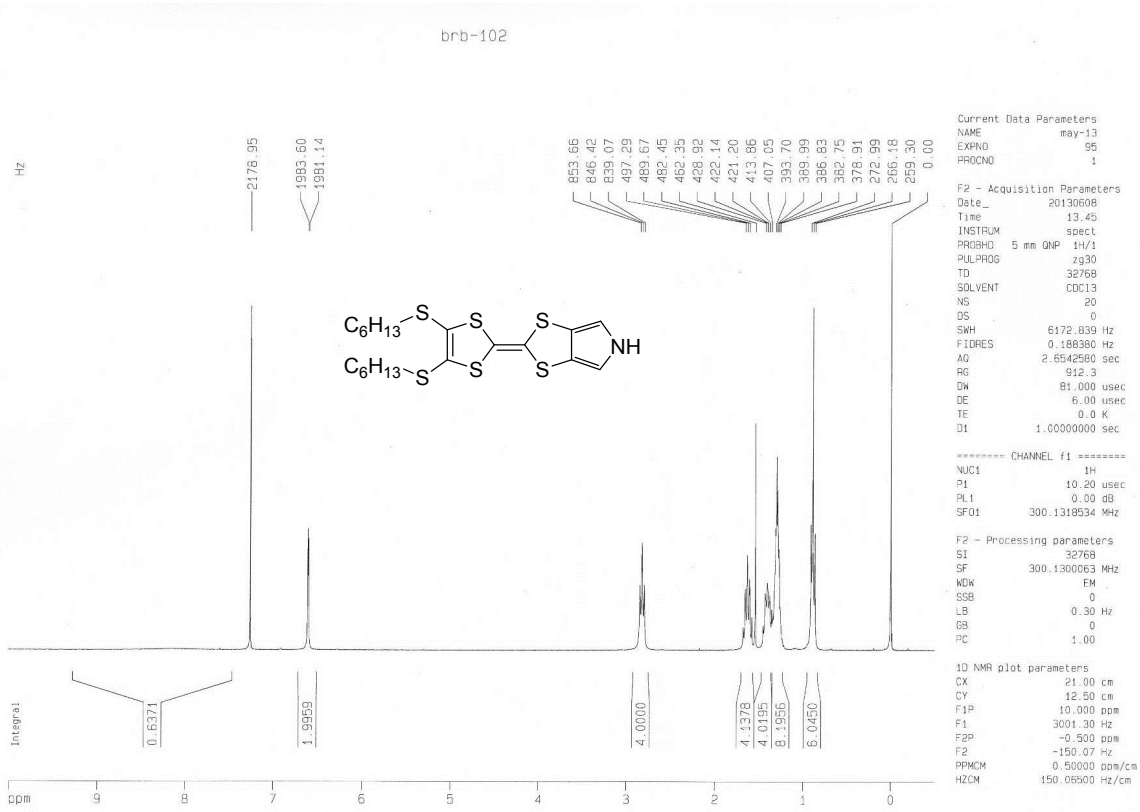

Figure S1. ^{1}H NMR spectrum of compound **7** in $CDCl_3$

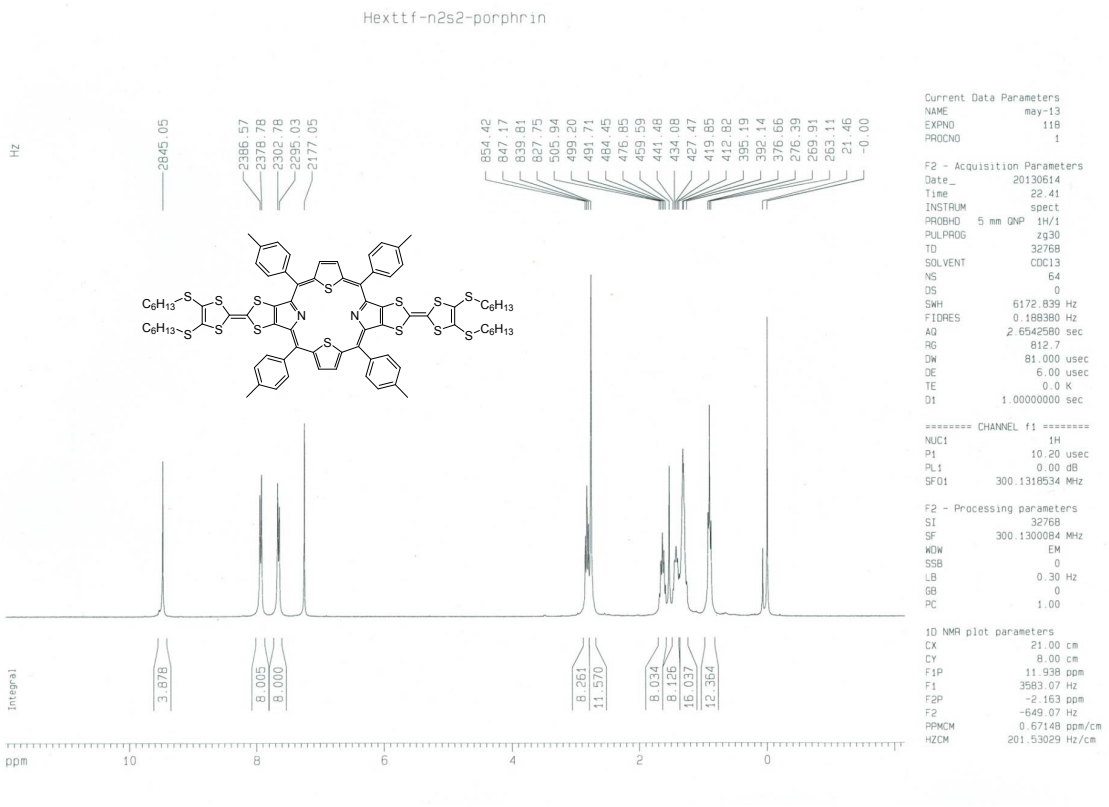

Figure S2. ^{1}H NMR spectrum of **1** recorded in $CDCl_3$

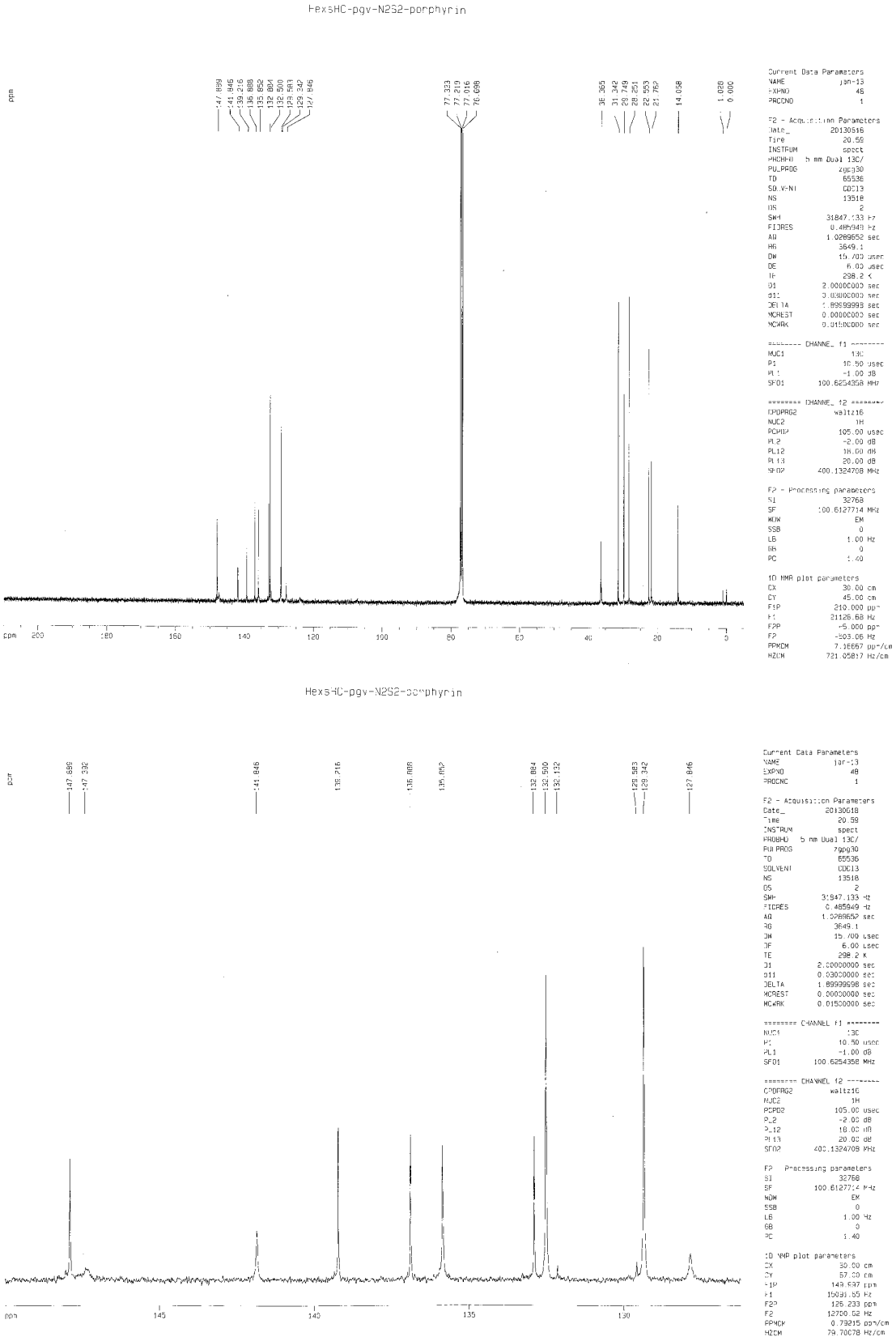

Figure S3. ^{13}C NMR (top) and its magnified (bottom) spectrum of **1** recorded in $CDCl_3$

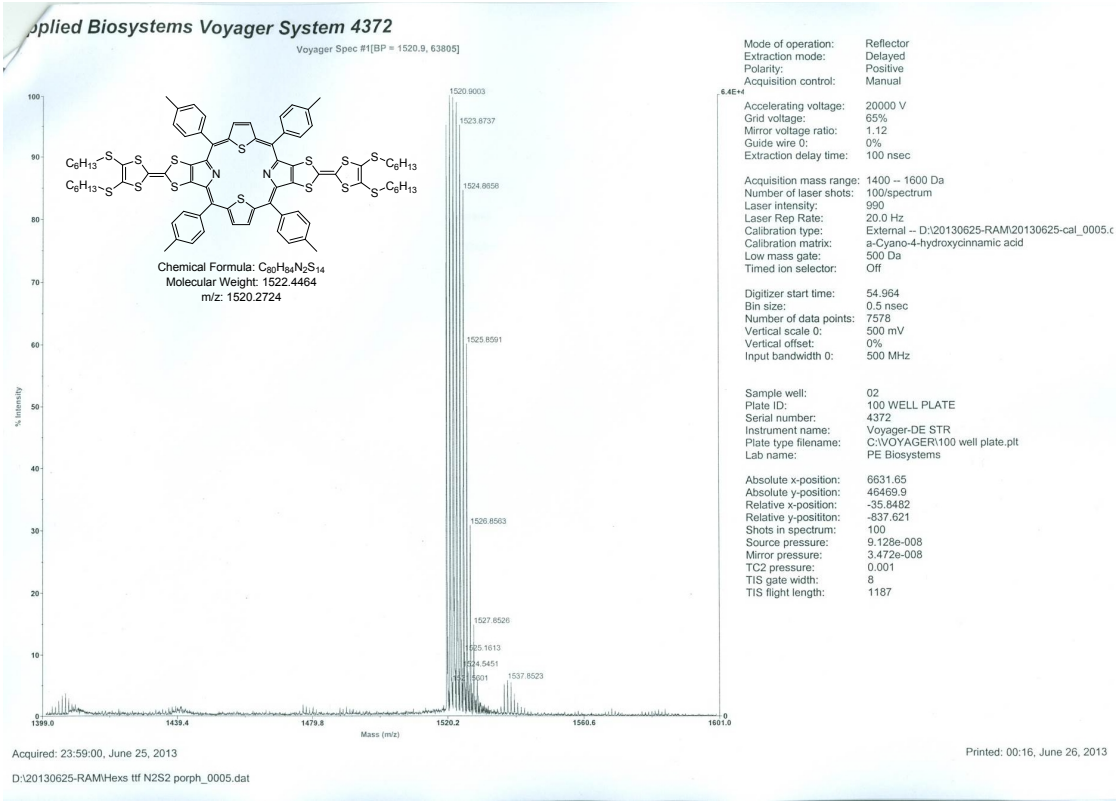

Figure S4. MALDI-TOF mass spectrum of compound **1**

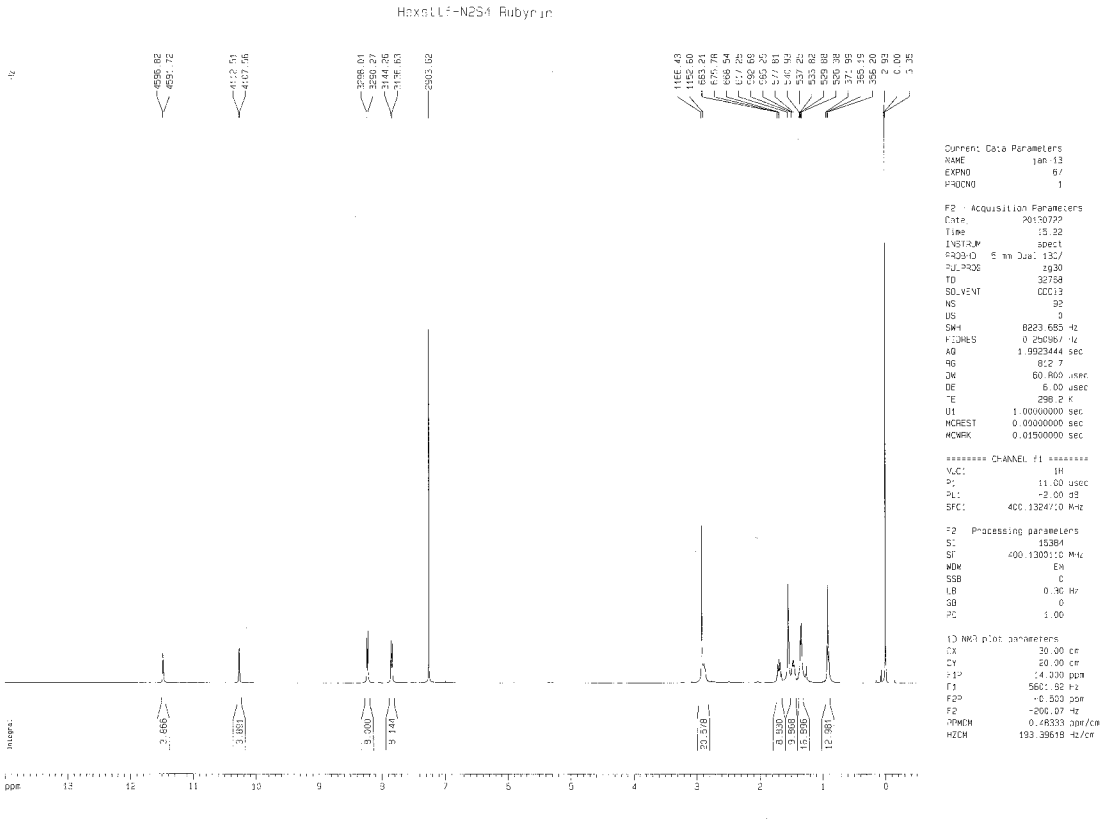

Figure S5. ^{1}H NMR spectrum of **2** recorded in $CDCl_3$

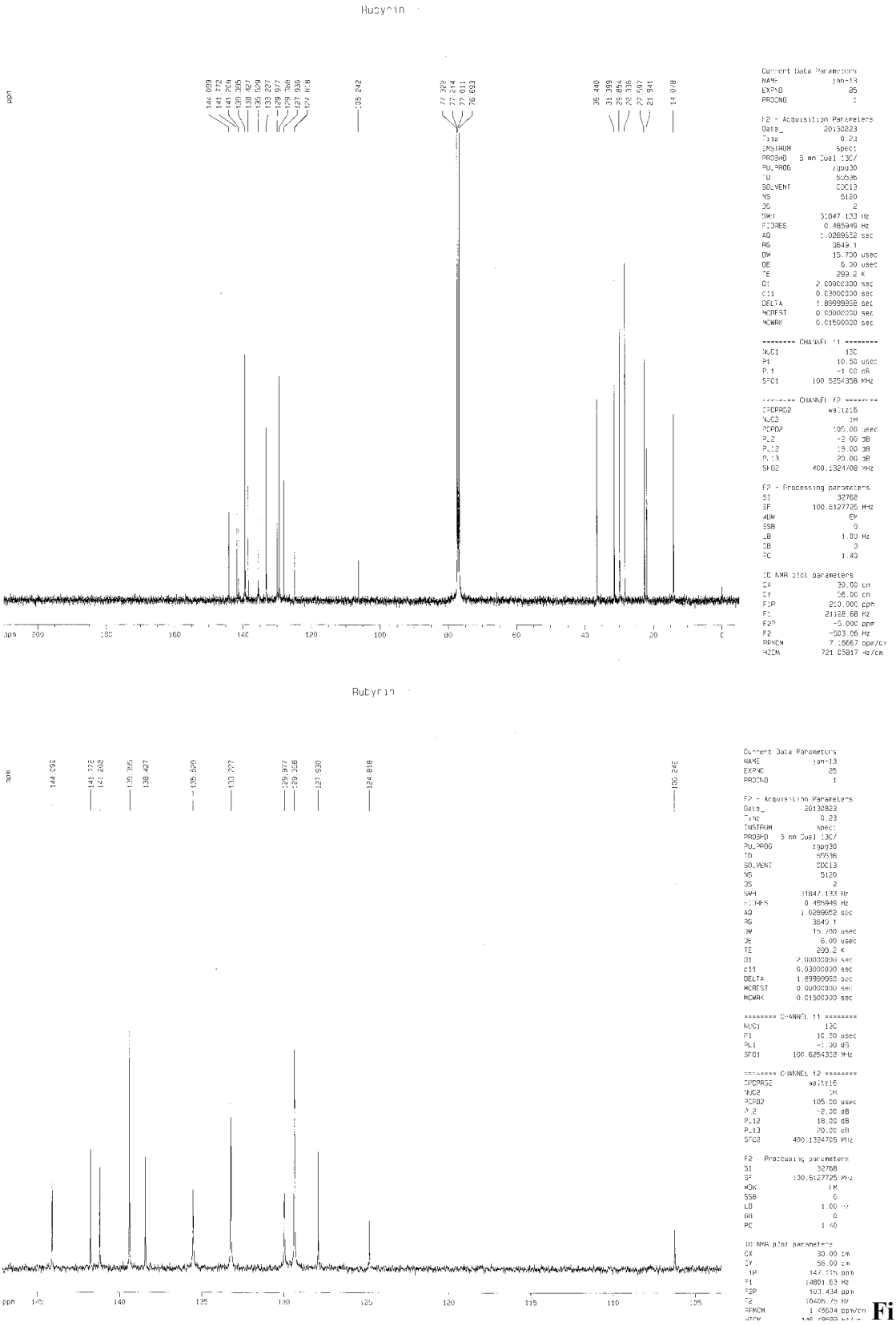

Figure S6. ^{13}C NMR (top) and the magnified (bottom) spectrum of **2** recorded in $CDCl_3$

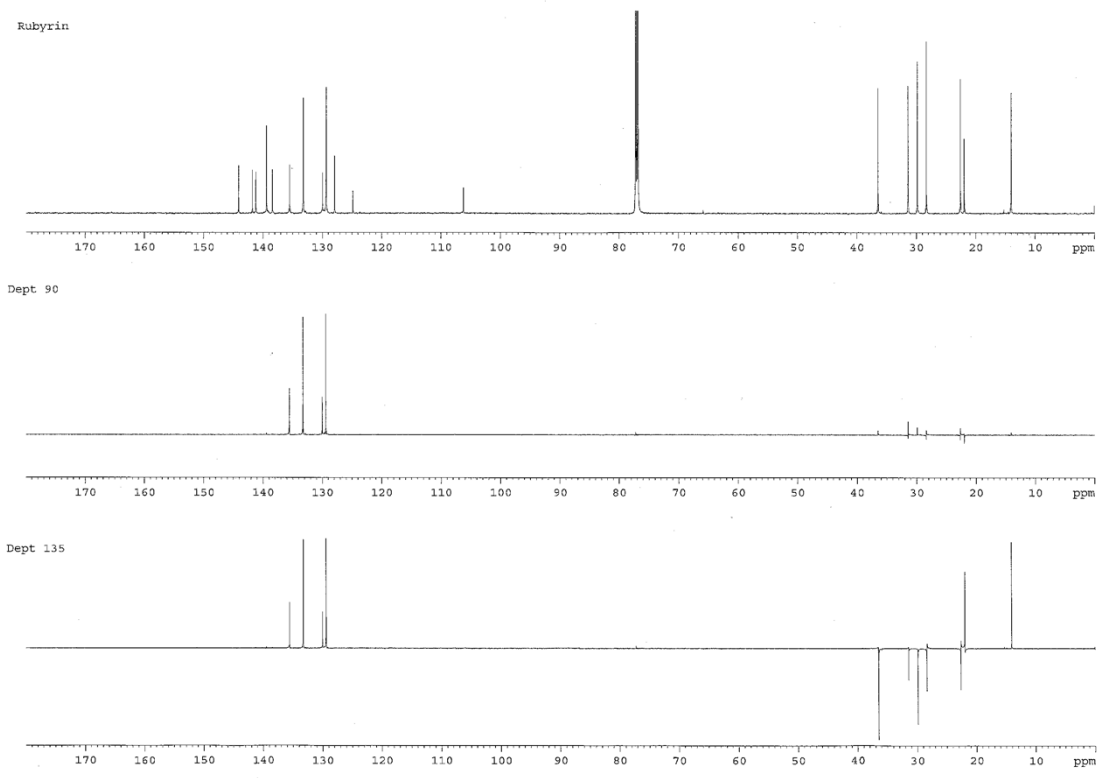

Figure S7. DEPT spectra of **2** recorded in $CDCl_3$

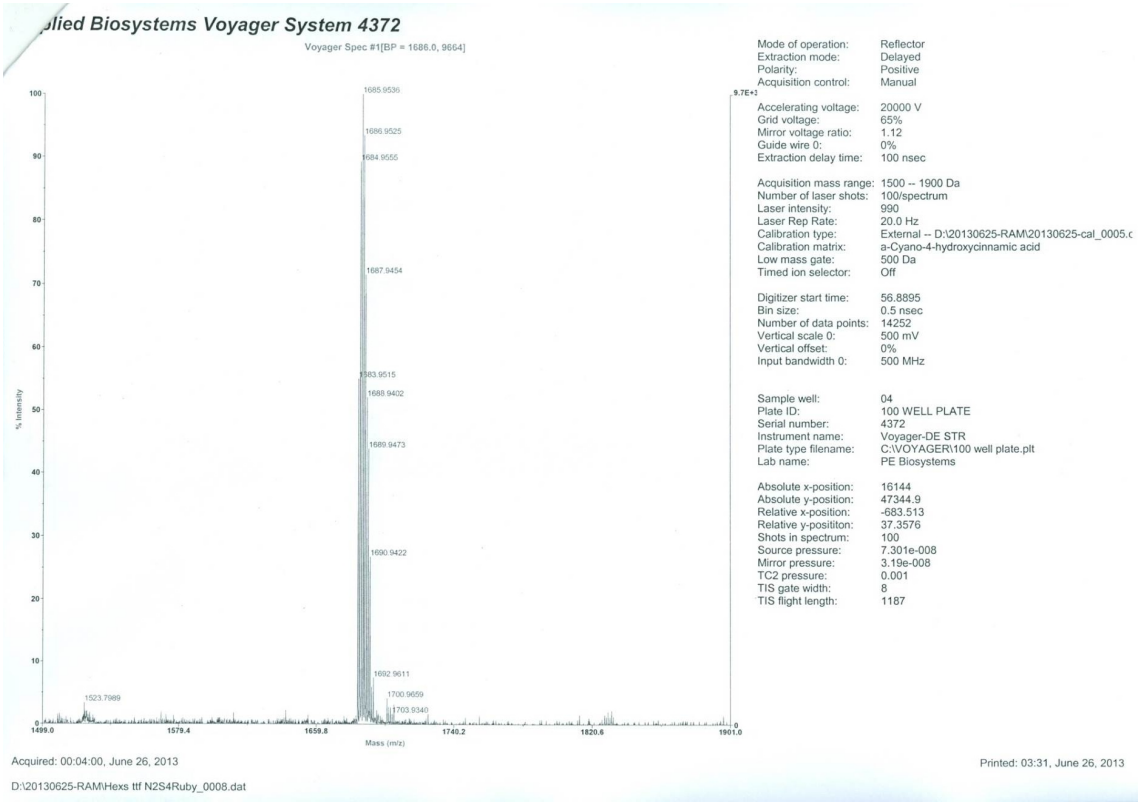

Figure S8. MALDI-TOF mass spectrum of compound **2**

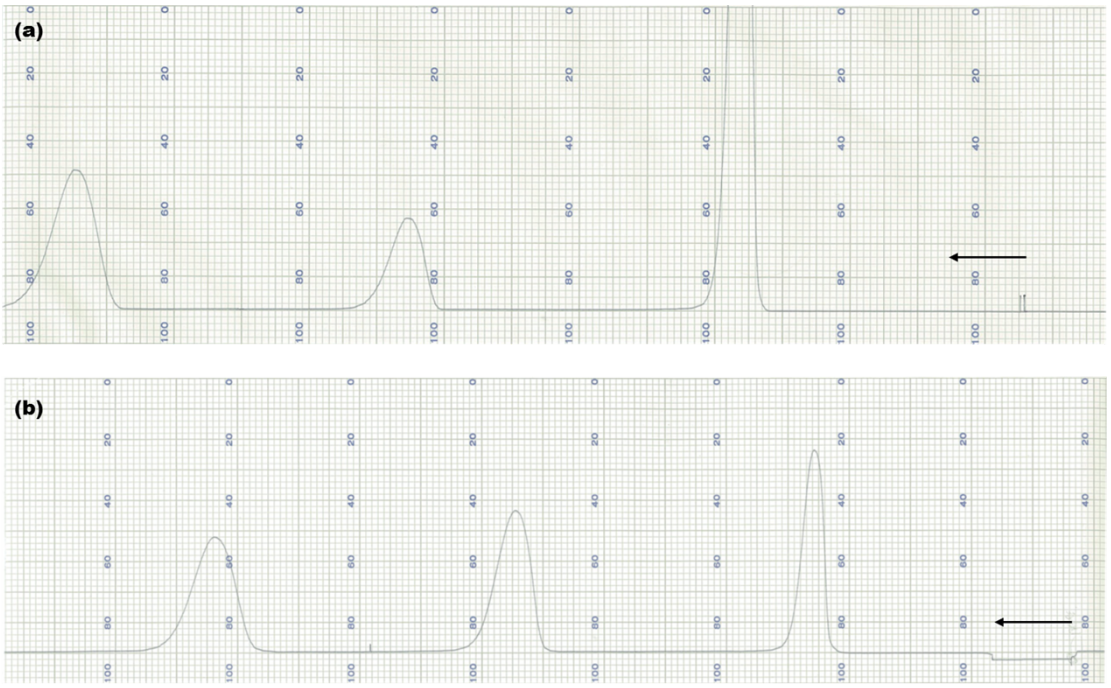

Figure S9. HPLC traces of (a) **1** and (b) **2** eluted by CH_2Cl_2 with flow rate of 4 mL/min.

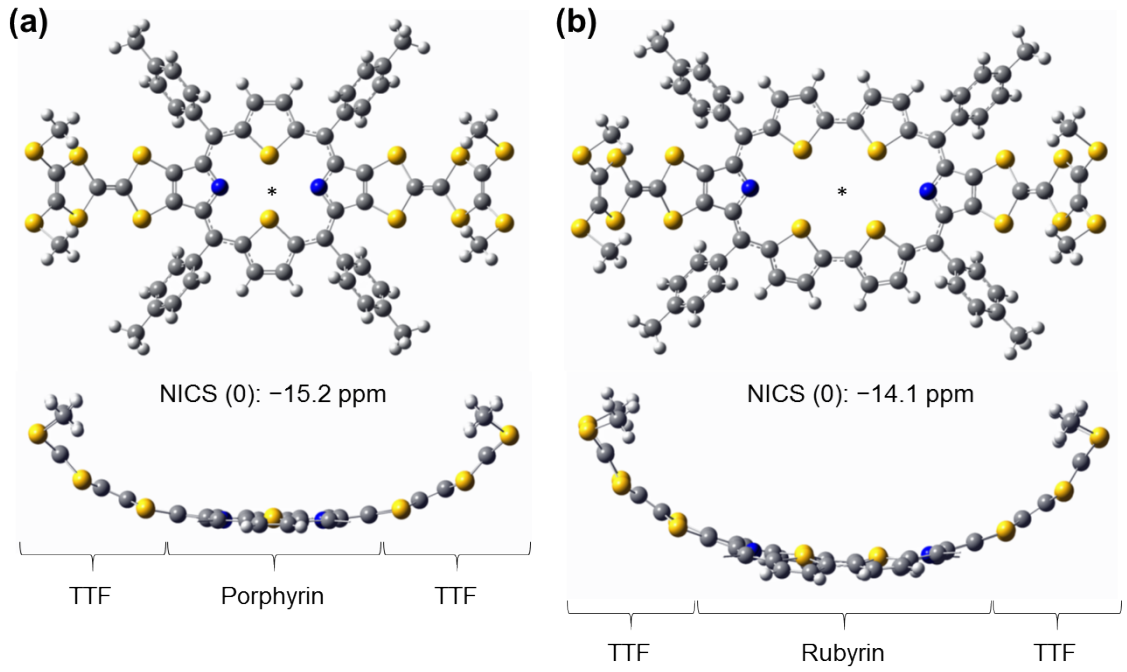

Figure S10. Ball-and-stick models of the optimized structures for (a) **1** and (b) **2** obtained by DFT calculations (B3LYP/6-31G*). NICS values are determined at the global center of the macrocycles, respectively.

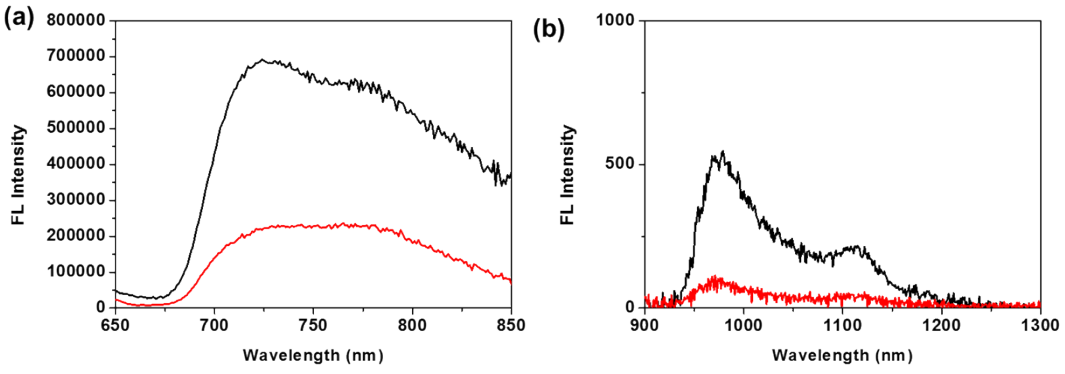

Figure S11. Comparative fluorescence spectra of (a) **1** and (b) **2** recorded in CH_2Cl_2 (black) and THF (red).

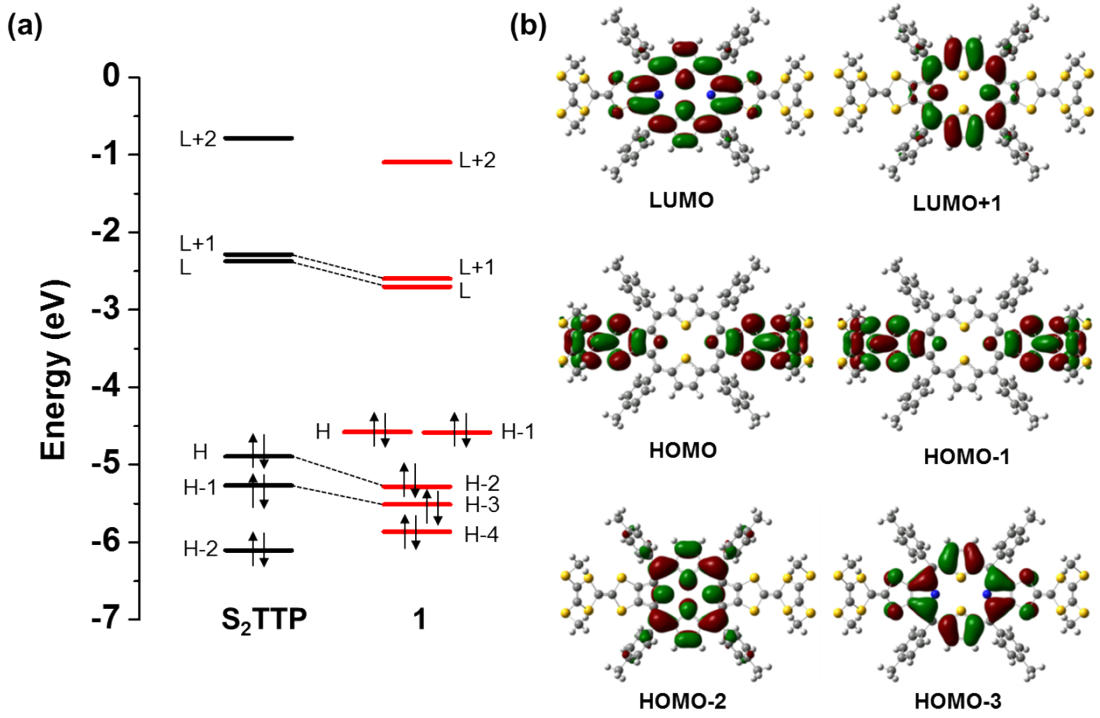

Figure S12. (a) Molecular orbital energy diagrams for **1** and **S_2TTP** obtained by B3LYP/6-31G* level calculations and (b) the selected frontier MO density maps of **1**.

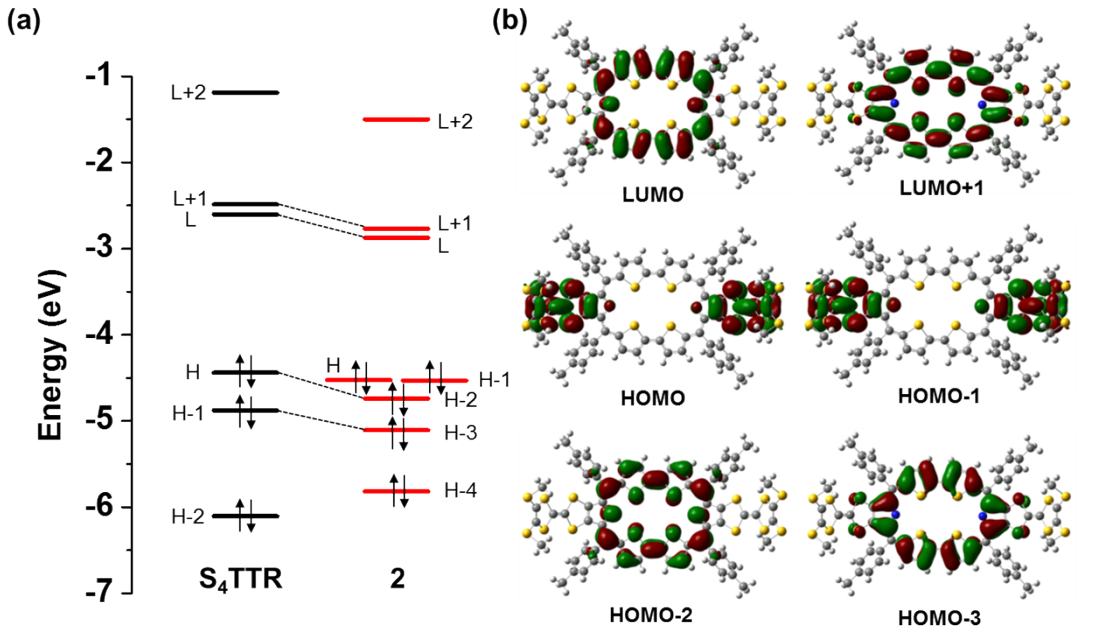

Figure S13. (a) Molecular orbital energy diagrams for **2** and **S_4TTR** obtained by B3LYP/6-31G*

level calculations and (b) the selected frontier MO density maps of **2**.

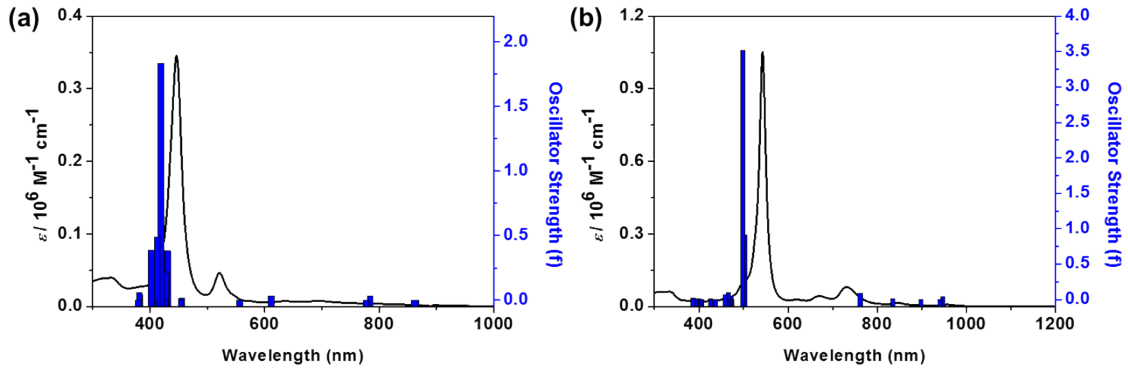

Figure S14. Simulated electronic states of (a) **1**, (b) **2** (c) $\mathbf{H_2 1^{2+}}$ and (d) $\mathbf{H_2 2^{2+}}$ obtained using TD-DFT calculations carried out at the B3LYP/6-31G* level.

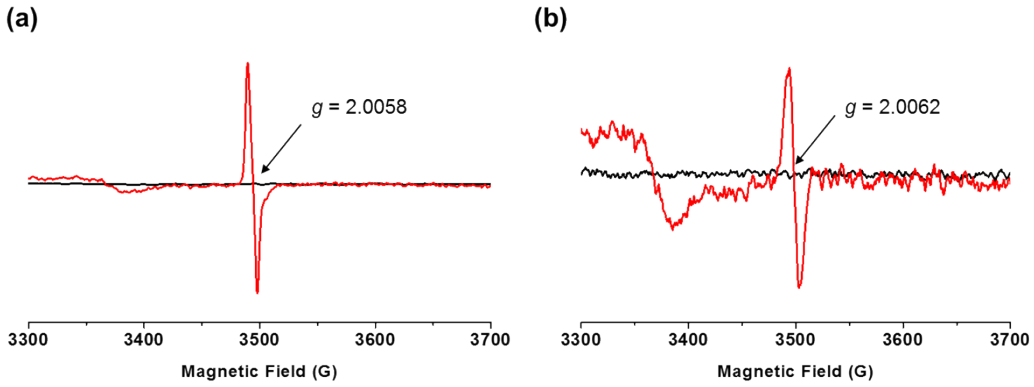

Figure S15. EPR spectra of (a) **1** recorded in CH_2Cl_2 under dark (black) and light irradication (red) and (b) **2** under dark (black) and light irradiation (red) conditions. [compound] = 0.1 mM.

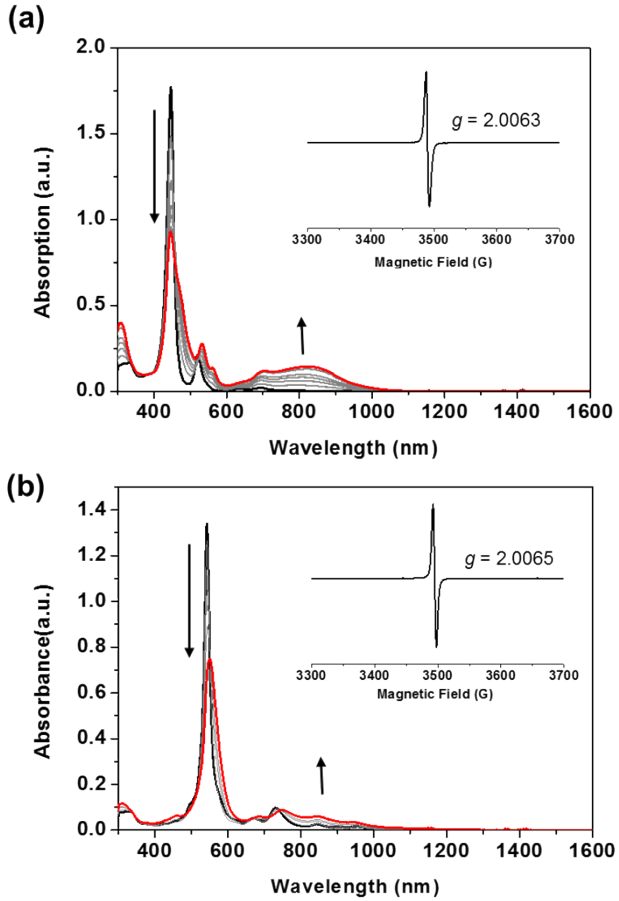

Figure S16. UV-vis-NIR absorption spectral changes upon chemical oxidation of (a) **1** and (b) **2** with *Magic Blue* in CH_2Cl_2. Insets show the EPR spectra of radical cation species of **1** and **2**, respectively.

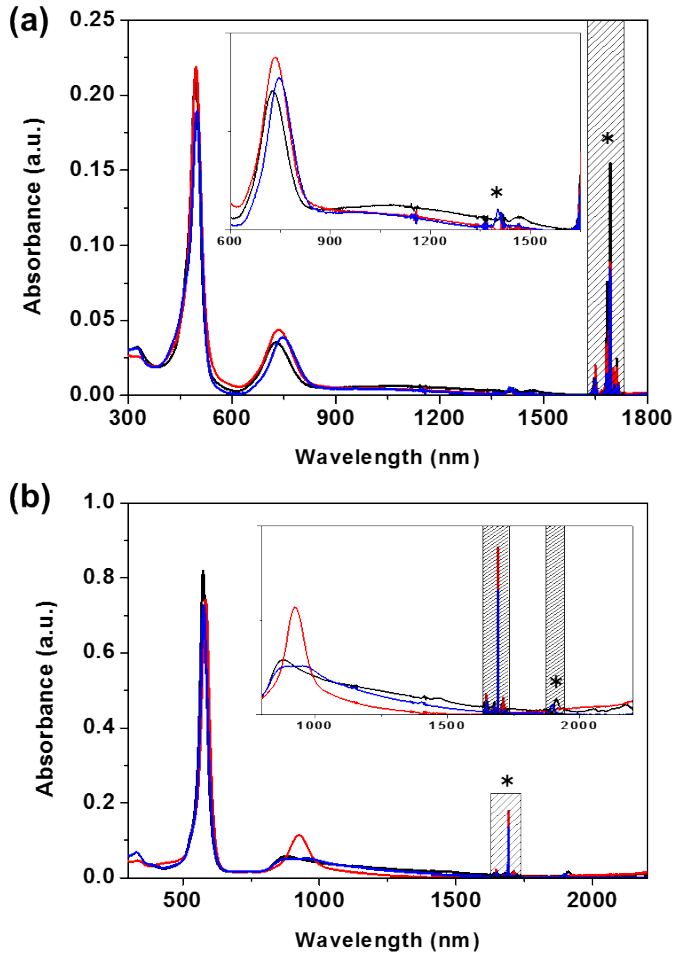

Figure S17. UV-vis-NIR spectra of (a) $\mathbf{H_2 1}^{2+}$ and (b) $\mathbf{H_2 2}^{2+}$ obtained using different acids; TFA (black), HCl (blue) and MSA (red) in CH_2Cl_2 solution. Asterisks indicate the solvent scattering peaks.

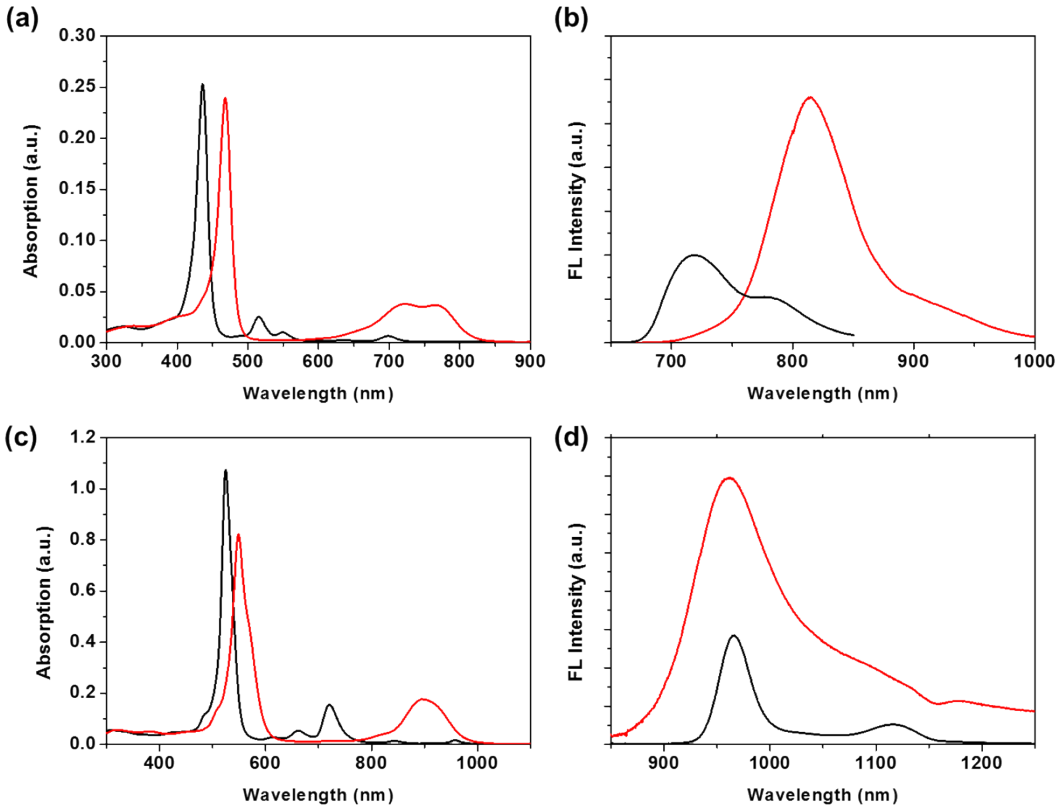

Figure S18. UV-vis-NIR absorption and emission spectra (black line) of reference compounds, (a, b) **S_2TTP** and (c, d) **S_4TTR** recorded in CH_2Cl_2, respectively. In the presence of TFA, the spectral changes of **S_2TTP** and **S_4TTR** were seen (red line).

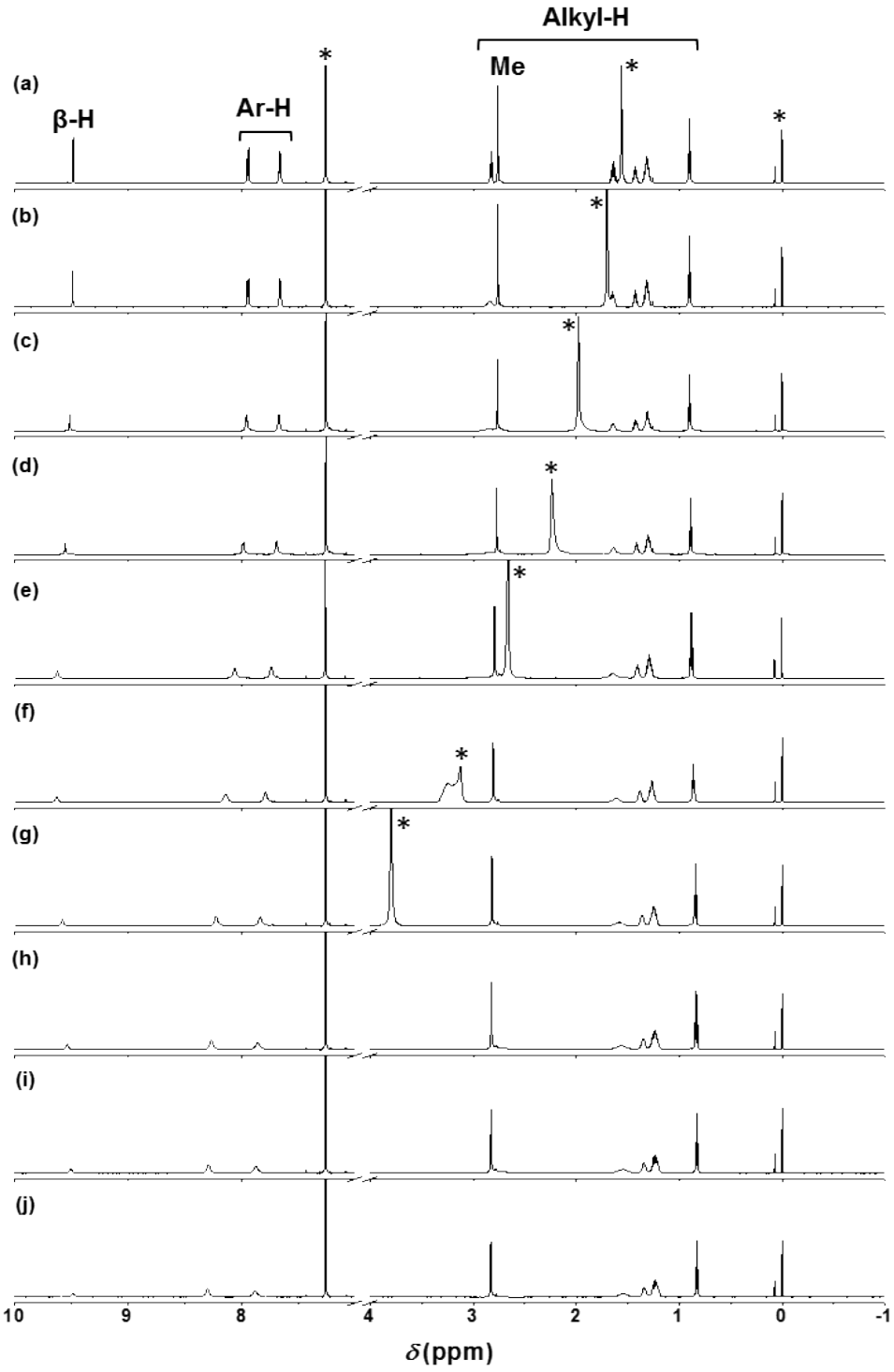

Figure S19. ^{1}H NMR spectral change of **1** in $CDCl_3$ upon addition of TFA. [TFA] = (a) 0 equiv. (b-j) 1-32 equiv. Asterisks indicate the residual solvent and impurities.

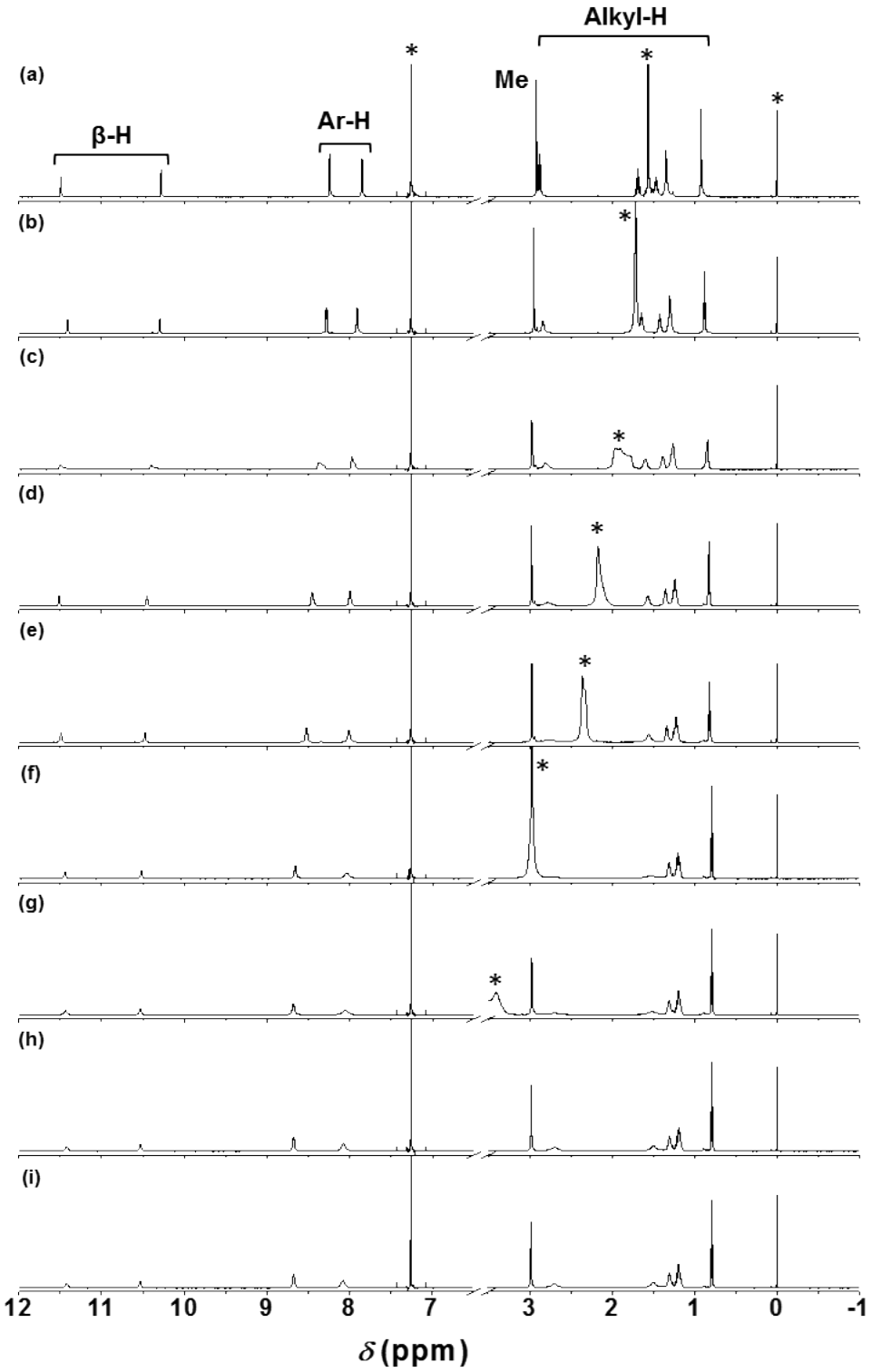

Figure S20. ^{1}H NMR spectral change of **2** in $CDCl_3$ upon addition of TFA. [TFA] = (a) 0 equiv. (b-j) 1-28 equiv. Asterisks indicate the residual solvent and impurities.

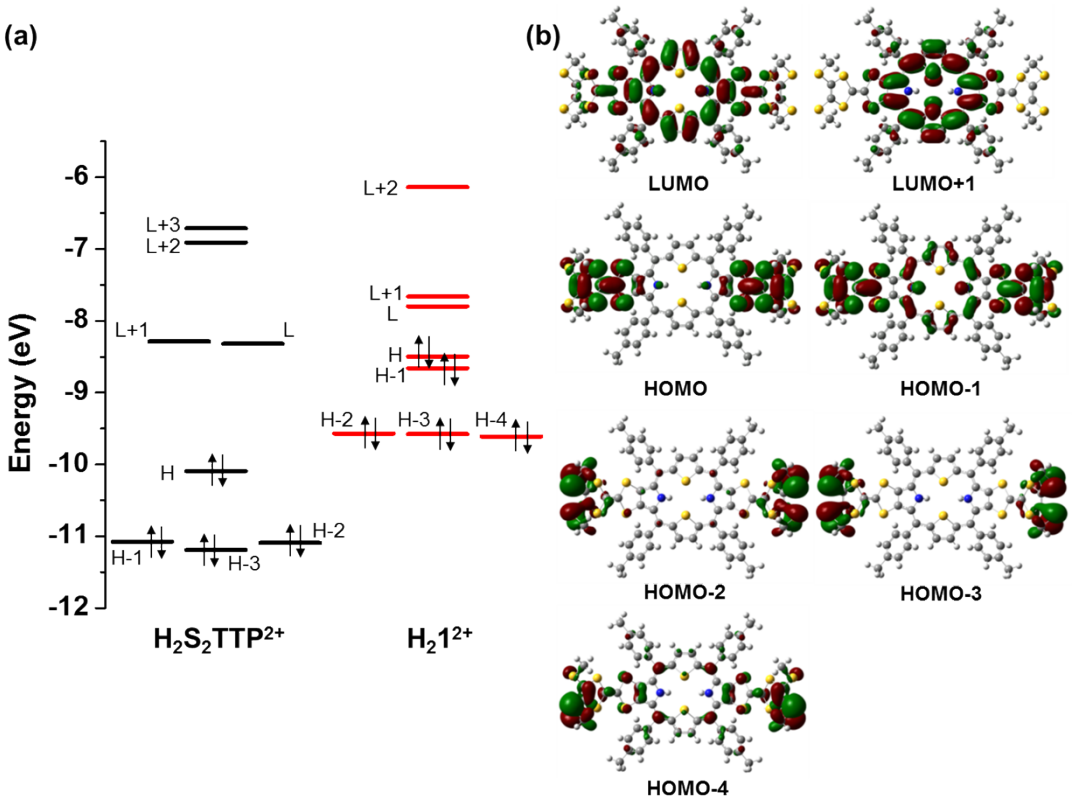

Figure S21. (a) Molecular orbital energy diagrams for $\mathbf{H_21^{2+}}$ and $\mathbf{H_2S_2TTP^{2+}}$ obtained by B3LYP/6-31G* level calculations and (b) the selected frontier MO density maps of $\mathbf{H_21^{2+}}$.

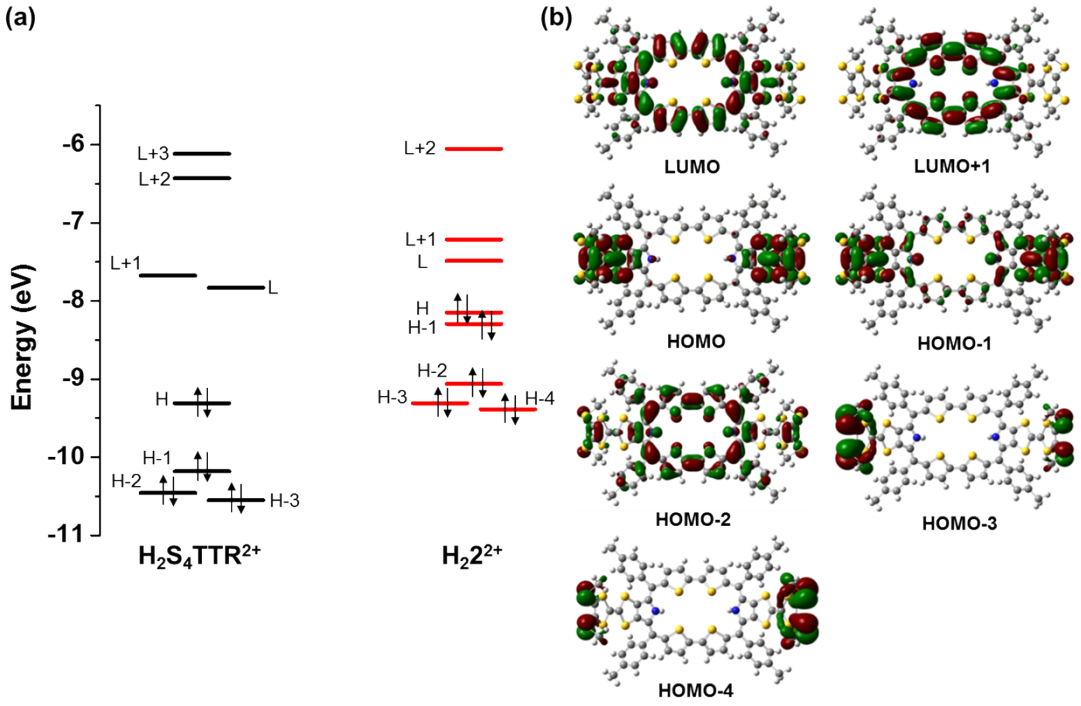

Figure S22. (a) Molecular orbital energy diagrams for $\mathbf{H_22^{2+}}$ and $\mathbf{H_2S_4TTR^{2+}}$ obtained by B3LYP/6-31G* level calculations and (b) the selected frontier MO density maps of $\mathbf{H_22^{2+}}$.

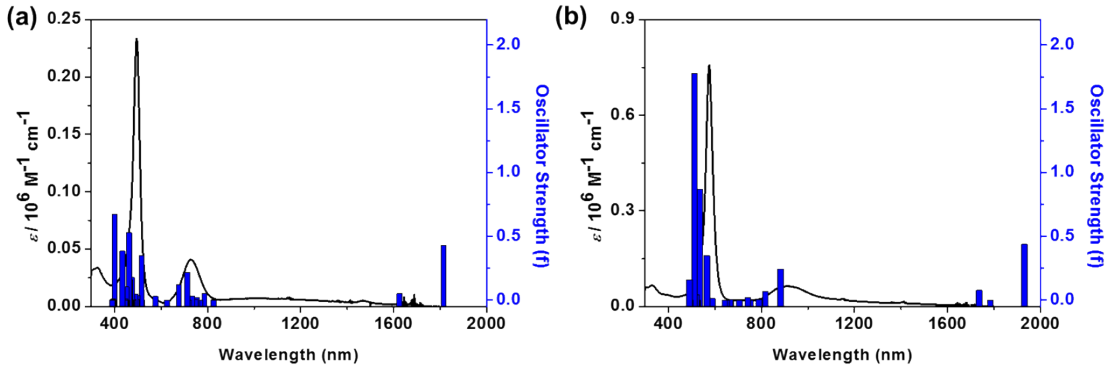

Figure S23. UV-vis-NIR absorption spectra (solid line) of $\mathbf{H_22^{2+}}$ and $\mathbf{H_21^{2+}}$ in CH_2Cl_2 along with the theoretical vertical excitation energies (blue bar) obtained from TD-DFT calculations at B3LYP/6-31g(d) level.